In Vivo Control of Soluble Guanylate Cyclase Activation by Nitric Oxide: A Kinetic Analysis

Peter Condorelli* and Steven C. George*†
*Department of Chemical and Biochemical Engineering and Materials Science, †The Center for Biomedical Engineering, University of California, Irvine, Irvine, California 92697-2575 USA

ABSTRACT Free nitric oxide (NO) activates soluble guanylate cyclase (sGC), an enzyme, within both pulmonary and vascular smooth muscle. sGC catalyzes the cyclization of guanosine 5′-triphosphate to guanosine 3′,5′-cyclic monophosphate (cGMP). Binding rates of NO to the ferrous heme(s) of sGC have been measured in vitro. However, a missing link in our understanding of the control mechanism of sGC by NO is a comprehensive in vivo kinetic analysis. Available literature data suggests that NO dissociation from the heme center of sGC is accelerated by its interaction with one or more cofactors in vivo. We present a working model for sGC activation and NO consumption in vivo. Our model predicts that NO influences the cGMP formation rate over a concentration range of ≈5–100 nM (apparent Michaelis constant ≈ 23 nM), with Hill coefficients between 1.1 and 1.5. The apparent reaction order for NO consumption by sGC is dependent on NO concentration, and varies between 0 and 1.5. Finally, the activation of sGC (half-life ≈ 1–2 s) is much more rapid than deactivation (≈50 s). We conclude that control of sGC in vivo is most likely ultra-sensitive, and that activation in vivo occurs at lower NO concentrations than previously reported.

INTRODUCTION

Nitric oxide (NO) plays key physiological roles as an intercellular messenger in such processes as modulation of blood flow, platelet inhibition, neurotransmission, regulation of smooth muscle tone, and host defense (Beckman and Koppenol, 1996; Denninger and Marletta, 1999; Ignarro et al., 1986, 1987; Malinski et al., 1993; Vaughn et al., 1998a; Wink and Mitchell, 1998). Because of the broad array of physiologic functions, NO is important to many organ systems, and a comprehensive understanding of its in vivo metabolism is critical.

NO is produced intracellularly in many different cell types by one of several isoforms of nitric oxide synthase. Once produced, NO can diffuse passively between cells; however, due to the presence of eleven valence electrons, it can also be rapidly consumed by several chemical reactions. In vivo, NO consumption can be approximated by three chemical reactions (Beckman and Koppenol, 1996): activation of soluble guanylate cyclase (sGC), rapid reaction with hemoglobin in blood, and oxidation by superoxide. The reaction with sGC is a proven signaling pathway for NO in which activated sGC catalyzes the conversion of guanosine 5′-triphosphate (GTP) to cyclic guanosine 3′,5′-monophosphate (cGMP). This pathway is the mechanism by which NO regulates smooth muscle tone, and thus local blood flow.

Although much is known about the reaction of NO with sGC, critical questions remain regarding the mechanism (including the in vivo concentration range) by which NO regulates the activity of sGC and the rate of NO consumption by this pathway. Experiments have been performed under nonphysiological conditions and in several different systems. In addition, there are explicit discrepancies in experimental and theoretical predictions regarding necessary and available free NO in vivo.

It has been reported that sGC is 50% activated at ≈250 nM NO (Stone and Marletta, 1996), which is much higher than NO concentrations predicted in arterial smooth muscle (Vaughn et al., 1998a,b). In vitro studies have reported half-lives for sGC deactivation that range from 1 to 9 min at physiological conditions (Brandish et al., 1998; Palmer et al., 1987). Finally, first- and second-order rate expressions (Vaughn et al., 1998b) do not correlate well with the experimental in situ monitoring of NO release and diffusion through smooth muscle (Malinski et al., 1993).

A missing link in our understanding of the reaction between NO and sGC has been a complete kinetic analysis under in vivo conditions. Herein, we convert available in vitro kinetic data into a comprehensive mathematical framework to provide a mechanism by which NO regulates sGC in vivo, as well as the consumption rate of NO resulting from this pathway. Ranges are determined for both the Hill coefficient, n_H, and apparent Michaelis constant, K_m. We conclude the following: 1) NO can control the activation of sGC in vivo over a concentration range of ≈5–100 nM; 2) intracellular thiol proteins, or other cofactors, play a critical role in the deactivation (and thus control) of sGC; 3) the activation of sGC is roughly an order of magnitude faster than deactivation; 4) the consumption of NO by this pathway is zero order for NO concentrations >200 nM; and 5)

Received for publication 17 November 2000 and in final form 9 February 2001.

Address reprint requests to Steven C. George, Dept. of Chemical and Biochemical Engineering and Materials Science, The Center for Biomedical Engineering, University of California, Irvine, Irvine, CA 92697-2575; Tel.: 949-824-3941; Fax: 949-824-2541; E-mail: scgeorge@uci.edu.

0006-3495/01/05/2110/10 $2.00

the Hill coefficient is ≥ 1, thus sGC is most likely an ultra-sensitive enzyme.

METHODS OF ANALYSIS

In mammals, sGC is a 150-kDa heterodimer, consisting of $\alpha 1$ (74–82 kDa) and $\beta 1$ (69–74 kDa) subunits (Brandish et al., 1998, Makino et al., 1999; Tomita et al., 1997). In the absence of NO, the prosthetic heme moiety is ligated by an axial histidine (His) residue, and exists as a five-coordinate histidyl complex (Denninger and Marletta, 1999; Stone and Marletta, 1994; Zhao et al., 1998a,b). This heme ligand has been identified as $\beta 1$-His-105, located 105 amino acid residues from the NH_2-terminus of the $\beta 1$ subunit (Zhao and Marletta, 1997; Zhao et al., 1998b). Free NO binds to the heme and can increase the activity of sGC up to 400-fold above basal (Stone and Marletta, 1995).

NO binding mechanism

A previous study (Stone and Marletta, 1996) investigated the activation of sGC by free NO in vitro under anaerobic conditions at 10°C, and proposed a complex NO binding mechanism. However, these experiments were affected by the presence of dithiothreitol, a di-thiol, which reacts with free NO in a manner similar to glutathione (GSH) and cysteine (Hogg et al., 1996; Wong et al., 1998).

Based on stopped-flow spectroscopy data obtained at 4°C with initial NO concentrations, $[NO]_{initial}$, in the range 570–500,000 nM, a simplified binding mechanism has been proposed (Zhao et al., 1999). This mechanism is depicted in Fig. 1 (*solid lines*) and assumes that sGC consists of a single fraction. In the first binding phase, the basal form of sGC, E_1, binds NO to form a 6-coordinate nitrosyl complex, E_2. In the second phase, E_2 is slowly converted to the 5-coordinate nitrosyl complex, E_3, by two parallel pathways (one NO-dependent and one NO-independent), as the axial histidine (His) bond to the heme iron (Fe) is broken. The NO-dependent pathway is characterized by the irreversible, second-order constant, k_3. We assumed that free NO participating in this reaction is decomposed to another species. We considered the NO-independent pathway to be reversible, as characterized by first-order constants, k_2 and k_{-2}. This mechanism provides the starting point for our model development. The apparent rate constants, quoted for NO binding at 4°C are: 0.14 $nM^{-1}s^{-1}$, 50 s^{-1}, 0.0087 s^{-1}, and 0.00024 $nM^{-1}s^{-1}$, for k_1, k_{-1}, k_2, and k_3, respectively (Zhao et al., 1999).

NO dissociation rates and mechanism

NO dissociation from sGC has been studied in vitro at temperatures of 20 and 37°C (Brandish et al., 1998; Kharitonov et al., 1997a,b; Magulis and Sitaramayya, 2000). Dissociation rate data has been expressed in terms of an observed pseudo-first-order rate constant, $k_{D,obs}$.

One laboratory used NO scavengers (i.e., hemoglobin or myoglobin) to maintain free NO concentrations at very low levels in solution, and observed that addition of GTP increased $k_{D,obs}$ from $6-8 \times 10^{-4}$ to $3-5 \times 10^{-2}$ s^{-1} at 20°C (Kharitonov et al., 1997a,b). This apparent GTP effect is consistent with a previous resonance Raman spectroscopy study (Tomita et al., 1997), and other recent data (Magulis and Sitaramayya, 2000). However, another study (Brandish et al., 1998) observed virtually no change in $k_{D,obs}$ upon addition of GSH and GTP.

We modified the most recent binding mechanism (Zhao et al., 1999) to include dissociation of NO from the E_3 form of sGC (*dashed lines* in Fig. 1). NO dissociation from sGC is characterized by the first-order rate constants k_{-2} and k_D. Recent data (Eu et. al., 2000) suggest that large protein thiols are an efficient sink or scavenger of NO to form nitrosothiols. In vivo, intracellular GSH concentrations can reach 10 nM, and large protein thiols are present at even higher concentrations. On this basis, we assumed that intracellular thiols are present in excess. Our modified mechanism assumes k_{-2} to account for NO dissociation from sGC in the absence of in vivo cofactors, and k_D for accelerated NO dissociation in vivo (Palmer et al. 1987). Any NO dissociating from sGC via the k_D pathway is assumed to be rapidly decomposed (Hogg et al. 1996, Wong et al. 1998). Although current experimental data cannot distinguish between dissociation of NO from E_3 to either E_2 or E_1, this mechanism is a starting point for simulation of sGC regulation by NO in vivo.

cGMP production

Different forms of sGC catalyze conversion of GTP to cGMP at different rates. The rate of cGMP formation, V_{cGMP}, depends upon the concentrations of the different forms of sGC, their respective turnover numbers, and upon NO concentration. The specific activity of sGC has been correlated in terms of the maximum reaction rate, V_{max}, and apparent Michaelis constant, $K_{m,GTP}$, with GTP as the substrate. In general, the apparent K_m is defined as the substrate concentration, which produces 50% of full enzyme activity (Stryer, 1995), but does not necessarily imply Michaelis–Menten kinetics. Apparent $K_{m,GTP}$ values for the basal and fully activated forms of sGC have been determined as 85–120 μM and 58 μM, respectively (Ignarro et al., 1982). Under in vivo conditions within smooth muscle, GTP is present in excess ([GTP] $\cong$1 mM = 1000 μM); thus, enzyme activity is independent of [GTP] (i.e., the dependence of V_{cGMP} on [GTP] can be ignored). Thus, under these conditions, we can write

$$\frac{d[cGMP]}{dt} = V_{cGMP} = k_{GCB}E_1 + k_{GC6}E_2 + k_{GC5}E_3, \quad (1)$$

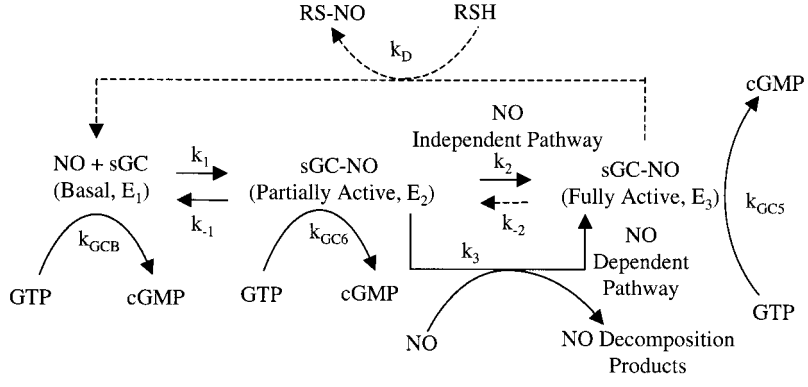

FIGURE 1 Proposed in vivo mechanism for the binding of free NO to sGC based on in vitro data (Zhao et al., 1999). *Solid lines*, experimentally observed phenomena; *dashed lines*, proposed features based on analysis of in vitro data, as characterized by rate constant, k_D.

where t is time (seconds), and k_{GCB}, k_{GC6}, and k_{GC5} are the turnover numbers (s^{-1}) for the basal, 6-coordinate nitrosyl and 5-coordinate nitrosyl forms of sGC, respectively (see Fig. 1). E_1, E_2, and E_3 (represented in matrix form by vector **E**, see Eq. 3) are the concentrations of sGC species (nM), subject to the constraint: $E_0 = E_1 + E_2 + E_3$, where E_0 represents the total sGC concentration.

Thus, computation of V_{cGMP} requires determination of E_1, E_2, and E_3, which, in general, are functions of time and space. However, if NO binding proceeds rapidly compared to cGMP formation, these enzyme concentrations may be expressed in terms of NO concentration, [NO].

NO consumption rates

Within smooth muscle, in vivo consumption of NO via reaction with sGC is coupled with the reduction of sGC-NO. Adding the decomposition rate of free NO to the rates of NO binding to forms E_1 and E_2 of sGC (see Fig. 1), we write

$$-\frac{d[NO]}{dt} = R_{NO} = k_1[NO]E_1 - k_{-1}E_2 + k_3[NO]E_2. \quad (2)$$

The first two terms of Eq. 2 represent the forward and reverse rates of NO consumption in the first binding phase, and the last term represents NO consumed by the NO-dependent pathway of the second binding phase (see Fig. 1).

Numerical methods

Assuming elementary reactions, transient mass balances on the sGC species for a well-mixed, constant-volume system, yield the matrix expression,

$$\frac{d\mathbf{E}}{dt} = \mathbf{A}_E\mathbf{E} + \mathbf{B}_E E_0. \quad (3)$$

The matrix, $\mathbf{A}_E$, and vector, $\mathbf{B}_E$, are derived from the mechanism depicted in Fig. 1.

If [NO] is maintained at a constant level within the cell, Eq. 3 can be integrated analytically to obtain a transient solution. If [NO] is a complex function of time, or depends strongly upon its consumption and diffusion rates in vivo, Eq. 3 must be integrated numerically. Under certain physiological conditions, the pseudo-steady-state approximation (PSSA) can be applied to the enzyme species (Bray and White, 1966). Although sGC is confined inside the cells, living matter otherwise constitutes an open system with a continuous supply of free NO and GTP, and continuous removal of cGMP. Hence, despite transient fluctuations in vivo, pseudo-steady-state should be attained rapidly under normal physiological conditions. Applying PSSA by setting the time derivatives to zero in Eq. 3, we obtain

$$\mathbf{E} = -\mathbf{A}_E^{-1}\mathbf{B}_E E_0, \quad (4)$$

where $\mathbf{A}_E^{-1}$ is the inverse of the matrix $\mathbf{A}_E$.

Simultaneous solution of Eq. 4 yields expressions for the individual enzyme species in terms of [NO] and the rate constants defined by Fig. 1. Substitution of these expressions into Eq. 2 yields the following expression for the NO consumption Rate, R_{NO}:

$$\Phi = \frac{R_{NO}}{R_{NO,max}} = \frac{([NO] + B_{NO})[NO]}{A_0 + A_1[NO] + [NO]^2}, \quad (5)$$

where $A_0 = ((k_{-1} + k_2)k_D + k_{-1}k_{-2})/k_1k_3$, $A_1 = ((k_1 + k_3)k_D + (k_2 + k_{-2})k_1)/k_1k_3$, and $B_{NO} = k_Dk_2/k_3(2k_D + k_{-2})$. As [NO] $\rightarrow \infty$, $R_{NO} \rightarrow R_{NO,max} = (2k_D + k_{-2})E_0$, the maximum possible NO consumption rate resulting from the activation of sGC. At [NO] = $[NO]_{\Phi,50} = K_{m,\Phi}$, the apparent Michaelis constant for NO consumption with NO as the substrate, $\Phi = R_{NO}/R_{NO,max} = 0.5$. $[NO]_{\Phi,10}$ and $[NO]_{\Phi,90}$ are defined as the NO concentrations for which $\Phi = 0.1$ and $\Phi = 0.9$, respectively. It will be shown that, at these concentration levels, R_{NO} undergoes its transition to zeroth order behavior.

Substituting appropriate expressions for the individual enzyme species into Eq. 1 yields the following expression for V_{cGMP}:

$$\Theta = \frac{V_{cGMP}}{V_{cGMP,max}} = \frac{\gamma_{GCB}A_0 + (\gamma_{GCB}B_B + \gamma_{GC6}B_6 + B_5)[NO] + [NO]^2}{A_0 + A_1[NO] + [NO]^2}, \quad (6)$$

where $B_B = k_D/k_1$, $B_6 = (k_D + k_{-2})/k_3$, $B_5 = k_2/k_3$, $\gamma_{GCB} = k_{GCB}/k_{GC5}$ and $\gamma_{GC6} = k_{GC6}/k_{GC5}$. For these coefficients, the subscript denotes the form of the enzyme (basal (B), 6-coordinate nitrosyl (6), and 5-coordinate nitrosyl (5) complexes). For [NO] = 0, the enzyme exists exclusively in its basal form, and $V_{cGMP,B} = k_{GCB}E_0$. As [NO] $\rightarrow \infty$, $V_{cGMP} \rightarrow V_{cGMP,max} = k_{GC5}E_0$, where $V_{cGMP,max}$ is the maximum possible cGMP formation rate. At [NO] = $[NO]_{\Theta,50} = K_{m,\Theta}$, the apparent Michaelis constant for cGMP production with NO as the substrate, $\Theta = V_{cGMP}/V_{cGMP,max} = 0.5$. We also define $[NO]_{\Theta,10}$ and $[NO]_{\Theta,90}$ as the NO concentrations for which $V_{cGMP} = 0.1V_{cGMP,max}$ and $V_{cGMP} = 0.9V_{cGMP,max}$, respectively. The concentration range between $[NO]_{\Theta,10}$ and $[NO]_{\Theta,90}$ represents the physiological range of control for sGC activation.

Statistical analysis and parameter estimation

We focused on the in vivo rate of NO consumption resulting from sGC activation alone by excluding side reactions of free NO with other species. From Eq. 5, the fractional (relative) NO consumption rate, $\Phi = R_{NO}/R_{NO,max}$, is a function of [NO] and the inputs (independent variables, X_j): k_1, k_{-1}, k_2, k_{-2}, k_3, and k_D. Similarly, from Eq. 6, the fractional (relative) cGMP formation rate, $\Theta = V_{cGMP}/V_{cGMP,max}$, also depends upon two additional inputs: $\gamma_{GCB} = k_{GCB}/k_{GC5}$ and $\gamma_{GC6} = k_{GC6}/k_{GC5}$. On this basis, outputs (dependent variables, Y_i) were selected for statistical analysis, as defined below. We assessed each output's sensitivity to the inputs by using the normalized or relative sensitivity, $S^r_{i,j} = (X_j/Y_i)(\partial Y_i/\partial X_j) = \partial(\ln Y_i)/\partial(\ln X_j)$, as an index (Doctor, 1989). $S^r_{i,j}$ represents the fractional change of Y_i per fractional change in X_j.

sGC regulation by NO in vivo can be characterized by the rate of transition from zero to maximal activity and the concentration at which this transition occurs. Thus, four outputs, each for Φ and Θ were evaluated: 1) the apparent Michaelis constants, $K_{m,\Phi}$ and $K_{m,\Theta}$; 2) the [NO] levels at 10% of maximum rate, $[NO]_{\Phi,10}$ and $[NO]_{\Theta,10}$; 3) the [NO] levels at 90% of maximum rate, $[NO]_{\Phi,90}$ and $[NO]_{\Theta,90}$; and 4) the Hill coefficients, $n_{H,\Phi}$ and $n_{H,\Theta}$. $n_{H,\Phi}$ and $n_{H,\Theta}$, are defined as the logarithmic slopes of $\Phi/(1 - \Phi)$ and $\Theta/(1 - \Theta)$ versus [NO], evaluated at $\Phi = 0.5$ and $\Theta = 0.5$, respectively (Stryer, 1995),

$$n_{H,\Phi} = \frac{[NO]}{[\Theta/(1-\Theta)]}\frac{\partial[\Theta/(1-\Theta)]}{\partial[NO]} = \frac{\partial \ln[\Theta/(1-\Theta)]}{\partial \ln[NO]}, \quad \text{at} \quad \Theta = 0.5. \quad (7)$$

$$n_{H,\Phi} = \frac{[NO]}{[\Phi/(1-\Phi)]}\frac{\partial[\Phi/(1-\Phi)]}{\partial[NO]} = \frac{\partial \ln[\Phi/(1-\Phi)]}{\partial \ln[NO]}, \quad \text{at} \quad \Phi = 0.5. \quad (8)$$

Typically, $n_H = 1$ for enzymes exhibiting Michaelis–Menten behavior, $n_H < 1$ for sub-sensitive enzymes, and $n_H > 1$ for ultra-sensitive enzymes (Stryer, 1995; Ferrell and Machleder, 1998; Koshland, 1998).

Table 1 summarizes the input parameter values assumed for this analysis. Each median value and standard deviation (SD), shown in Table 1, corresponds to the 50-percentile and square root of the variance for each assumed distribution, respectively. Gaussian distributions were established for $\gamma_{GCB} = k_{GCB}/k_{GC5}$ and $\gamma_{GC6} = k_{GC6}/k_{GC5}$, from our analysis of specific activity data (Brandish et al., 1998; Makino et al., 1999; Tomita et al., 1997; Stone and Marletta, 1995, 1998; Zhao et al., 1999). The activity of the 6-coordinate complex was assumed to be intermediate between that of the basal and 5-coordinate nitrosyl forms of sGC, based on our analysis of in vitro data (Zhao et al., 1999). It is important to note that Θ and Φ are independent of E_0, which is not well characterized. However, k_{GC5} has been measured in vitro by several investigators at various enzyme concentrations (Brandish et al., 1998; Makino et al., 1999; Tomita et al., 1997; Stone and Marletta, 1995, 1998; Zhao et al., 1999).

The upper limit assumed for $k_{D,obs}$ with dithiothreitol and GTP both present, was 0.05 s^{-1} at 20°C (Kharitonov et al., 1997a,b), which corresponds to 0.2 s^{-1} at 37°C, based on the rate constant doubling for every 10°C rise in temperature (Bray and White, 1966). Referring to Fig. 1, it can be verified algebraically that $k_{D,obs} \cong k_D + k_{-2}$. Hence, k_{-2} was estimated as 0.002 ± 0.002 s^{-1} (SD) at 37°C from appropriate dissociation rate data (Brandish et al., 1998; Kharitonov et al., 1997a,b; Magulis and Sitaramayya, 2000). Similar analysis confirms the upper limit: $k_D \cong k_{D,obs} = 0.2$ s^{-1} at 37°C. The lower limit for k_D was taken as zero, because one study reported no increase in NO dissociation rates when GSH or GTP were added (Brandish et al., 1998). The assumed mean, $k_D \cong k_{D,obs} = 0.01$ s^{-1} at 37°C, was based on in vivo experiments (Palmer et al., 1987), which involved the NO-induced relaxation/contraction of rabbit aorta. The logarithm of k_D was assumed to be uniformly distributed between its median (0.01 s^{-1}) and upper limit (0.2 s^{-1}), respectively. k_D was varied between its upper and lower limits in assessing the dependence of Φ and Θ upon [NO].

To assess uncertainty, we extrapolated rate constants from 4 to 37°C by applying the Arrhenius equation (Bray and White, 1966):

$$k_i = k_{i0}\exp[-(E_{ai}/R)(1/T - 1/T_0)], \quad (9)$$

where subscript i denotes a step of the binding process (see Fig. 1), E_{ai} is the activation energy (J/mol) and R is the ideal gas law constant. T and T_0 are the absolute temperatures, 277 and 310 K, respectively. Eq. 9 was also applied to the reverse reactions by replacing i with $-i$. Based on literature data for similar reactions (Bray and White, 1966), E_{ai} was fitted to a normal distribution in the range, 13 ± 6 kcal/mol (55 ± 25 kJ/mol) (SD). k_i was then computed from E_{ai} ($i = 1, 2, 3, -1$).

As shown in Table 1, the uncertainties associated with the rate constants are high due to their exponential dependence upon the activation energies. Therefore, temperature extrapolation represents a potential source of error. In addition, the temperature dependence of the equilibrium constant for the first binding phase, $K_1 = k_1/k_{-1}$, is not well characterized, because the heat of reaction is unknown and appropriate data is available only at 4°C (Zhao et al., 1999). From the literature values quoted (Zhao et al., 1999) and the input parameter values summarized in Table 1, the corresponding median value is $K_1 = 0.14\ nM^{-1}s^{-1}/50\ s^{-1} \cong 2\ nM^{-1}s^{-1}/600\ s^{-1} \cong 0.003\ nM^{-1}$. Thus, this analysis assumes that K_1 is independent of temperature, which is equivalent to zero heat of reaction. In reality, we would expect K_1 to decrease or increase with temperature for an exothermic or endothermic reaction, respectively (Bray and White, 1966).

We applied Latin hypercube sampling (LHS) (McKay et al., 1979) to estimate the probability density functions for each output (D'Agostino and Stephens, 1986; Greenwood and Nikulin, 1996; Mendenhall and Scheaffer, 1973; Silverman, 1986). LHS was used to select 1000 unique combinations of the eight inputs listed in Table 1. Each combination was chosen to be of equal probability based on the assumed input distribution functions (see Table 1). Probability density functions for the outputs were determined by making preliminary nonparametric estimates (Mendenhall and Scheaffer, 1973; Silverman, 1986), followed by parametric correlation to standard probability distribution families (D'Agostino and Stephens, 1986; Greenwood and Nikulin, 1996; Mendenhall and Scheaffer, 1973).

TABLE 1 Input parameter values assumed for in vivo sensitivity analysis

Input	Units	Median	SD*
γ_{GCB} [#]	—	0.004	0.002
γ_{GC6} [#]	—	0.5	0.3
k_D [§]	s^{-1}	0.01	0.01
k_1 [¶]	$nM^{-1}s^{-1}$	2.0	2.0
k_2 [¶]	s^{-1}	0.1	0.1
k_3 [¶]	$nM^{-1}s^{-1}$	0.003	0.003
k_{-1} [¶]	s^{-1}	600.0	600.0
k_{-2} [¶,‖]	s^{-1}	0.002	0.002

*SD = standard deviation.
[#]Gaussian distribution.
[§]Logarithm of k_D uniformly distributed (upper limit = 0.2 s^{-1}, lower limit = 0).
[¶]Ea_1, Ea_2, Ea_3, Ea_{-1}, and Ea_{-1} normally distributed around 55 ± 25 kJ/mol (Eq. 9).
[‖]Based on dissociation rate data at 20–37°C (Brandish et al., 1998; Kharitonov et al., 1997a,b; Magulis and Sitaramayya, 2000).

Transient activation of sGC by NO

An exact simulation of sGC activation in vivo requires numerical integration of Eq. 3, and a mathematical description of both diffusion rates and NO consumption resulting from species other than sGC. We considered two simplified scenarios in which the level of NO was abruptly changed everywhere within the cell at initial conditions ($t = 0$) from [NO] = 0 to 500 nM (sGC activation) and from 500 nM to 0 (sGC deactivation). Initial conditions for the enzyme species were determined from Eq. 4. Eq. 3 was integrated to determine $E(t)$, with the resulting expressions substituted into Eq. 1, to determine $V_{cGMP}(t)$. $V_{cGMP}(t)$ was normalized to the function, $\theta(t) = (V_{cGMP}(t) - V_{cGMP,B})/(V_{cGMP,500} - V_{cGMP,B})$, where $V_{cGMP,500}$ is the steady-state rate of cGMP formation at [NO] = 500 nM, as determined from Eq. 6. $\theta(t)$ was plotted as a function of time for both the activation and deactivation scenarios with $k_D = 0$, 0.01, and 0.2 s^{-1}.

Dimensionless representation

From Eqs. 6 and 7, the Hill coefficient for cGMP formation, $n_{H,\Theta}$, and dimensionless Michaelis constant, $Y_{m,\Theta} = K_1K_{m,\Theta}$, may be expressed in terms of five dimensionless variables, $\alpha = k_2/(k_D + k_{-2})$, $\beta = k_3/[K_1(k_D + k_{-2})]$, $\epsilon = k_D/k_{-1}$, γ_{GCB}, and γ_{GC6}, as

$$n_{H,\Theta} = \frac{(1 - 2\gamma_{GCB})(v + x_\Theta^2)}{(1 - \gamma_{GCB})[v + 2(u + \alpha)x_\Theta] + 2(\gamma_{GC6} - \gamma_{GCB})x_\Theta}, \quad (10)$$

$$Y_{m,\Theta} = \frac{x_\Theta}{2\beta}, \quad (11)$$

where $K_1 = k_1/k_{-1}$, $u = (1 - 2\gamma_{GCB})\epsilon\beta + 1 - 2\gamma_{GC6} - \alpha$, $v = 4(1 - 2\gamma_{GCB})(1 + \epsilon\alpha)\beta$, and $x_\Theta = u + (u^2 + v)^{1/2}$.

For the median input parameter values summarized in Table 1 $\alpha \cong 10$, $\beta \cong 100$, $\epsilon \cong 1.5 \times 10^{-5}$, $\gamma_{GC6} = 0.5$, and $\gamma_{GCB} = 0.004$. In general, for the two-phase binding mechanism proposed, $n_{H,\Theta}$ must lie in the range $0 < n_{H,\Theta} < 2$. For Michaelis–Menten kinetics, $n_{H,\Theta} = 1$. It can be verified that

sGC approaches Michaelis–Menten behavior if $\beta = 0$. Other, nontrivial values of the dimensionless variables, for which $n_{H,\Theta} \rightarrow 1$, also exist.

RESULTS

cGMP formation and NO consumption

Figures. 2 *A* and 3 *A* depict Θ and Φ, respectively, as functions of [NO] in vivo, for $k_D = 0$, 0.01, and 0.2 s^{-1}. Θ is a monotonically increasing function of NO over a concentration range of 0.1–1000 nM depending on the value of k_D. From inspection of Figs. 2 *A* and 3 *A*, the values for $[NO]_{\Theta,10}$, $K_{m,\Theta}$, $[NO]_{\Theta,90}$, $[NO]_{\Phi,10}$, $K_{m,\Phi}$, and $[NO]_{\Phi,90}$ at the median values of the input parameters are roughly 5, 30, 90, 10, 50, and 200 nM, respectively. Figures 2 *B* and 3 *B* depict the logarithmic slopes as a function of [NO] (fractional change of Θ and Φ per fractional change in [NO], or the relative sensitivities $S^r_{\Theta,[NO]}$ and $S^r_{\Phi,[NO]}$, respectively). $S^r_{\Phi,[NO]}$ may be interpreted as the apparent reaction order of NO consumption with respect to [NO]. From inspection of these figures, the Hill coefficients, $n_{H,\Theta}$ and $n_{H,\Phi}$, are both $\approx$1.1, 1.3, and 1.5, with $k_D = 0$, 0.01, and 0.2 s^{-1}, respectively.

Statistical analysis

We identified the reaction rate constants (k_D, k_1, k_2, k_3, and k_{-1}) as important input parameters, with k_{-2} also playing a minor role, based on sensitivity analysis. The Michaelis constants are significantly more sensitive to k_D than the Hill coefficients. The sensitivities of both $n_{H,\Theta}$, and $K_{m,\Theta}$, with respect to γ_{GCB}, were found to be negligible. The relative

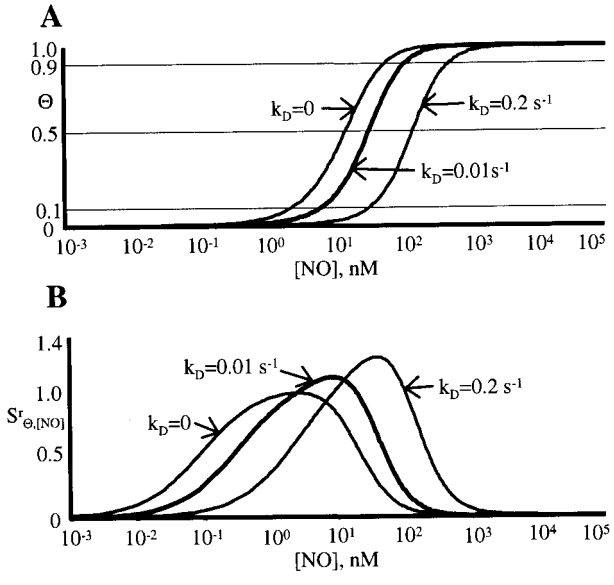

FIGURE 2 (*A*) Relative cGMP formation rate, $\Theta = V_{cGMP}/V_{cGMP,max}$, and (*B*) the logarithmic slope, $S^r_{\Theta,[NO]}$, as a function of [NO]. The logarithmic slopes correspond to apparent reaction orders with respect to [NO].

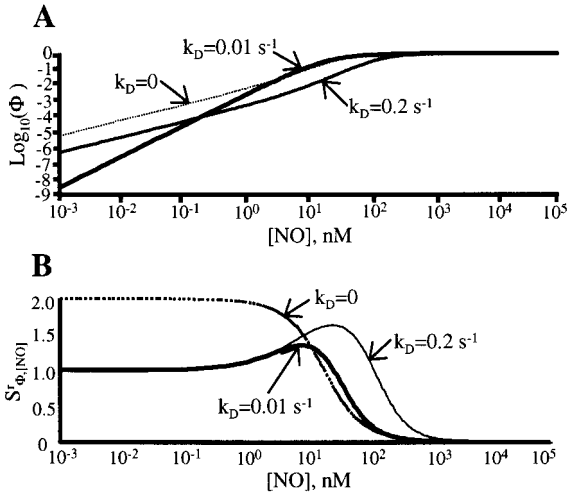

FIGURE 3 (*A*) Relative NO consumption rate, $\Phi = R_{NO}/R_{NO,max}$, and (*B*) the logarithmic slope, $S^r_{\Theta,[NO]}$, as a function of [NO]. The logarithmic slopes correspond to apparent reaction orders with respect to [NO].

sensitivities of all outputs to k_1 and k_{-1}, were equal in magnitude but opposite in sign (data not shown), which suggests that their dependence on these two parameters may be expressed in terms of the equilibrium constant, K_1.

In Table 2, the means (expected values) and percentiles are summarized for the eight outputs corresponding to cGMP formation and NO consumption rates, as estimated from LHS (McKay et al., 1979) using the input parameter values listed in Table 1. Expected values were computed from the estimated probability density functions, and percentiles were determined directly from LHS results.

In Fig. 4, *A*—*D*, is depicted the probability density functions, $f(Y_i)$, estimated for the eight outputs. $f(n_{H,\Theta})$ (Fig. 4 *A*) was correlated to the Weibull distribution on two intervals (D'Agostino and Stephens, 1986). $f(n_{H,\Phi})$ (Fig. 4 *B*) was correlated as a gamma distribution (D'Agostino and Stephens, 1986; Greenwood and Nikulin, 1996; Mendenhall and Scheaffer, 1973; Silverman, 1986). Quartile values of the Hill coefficients are indicated in Fig. 4, *A* and *B*. $f(n_{H,\Theta})$ is characterized by its abrupt peak at $n_{H,\Theta} = 1$. Despite the high likelihood at $n_{H,\Theta} = 1$, nearly 90% of the area under the $f(n_{H,\Theta})$ curve lies in the region where $n_{H,\Theta} > 1$, suggesting ultra-sensitive behavior. In contrast, $f(n_{H,\Phi})$ is much flatter, with only 70% of the curve area in the region where $n_{H,\Phi} > 1$. The median values for both $n_{H,\Theta}$ and $n_{H,\Phi}$ are about the same ($\cong$1.3) with mean (expected) values of 1.36 and 1.27, respectively.

$[NO]_{\Theta,10}$, $K_{m,\Theta}$, $[NO]_{\Theta,90}$, $[NO]_{\Phi,10}$, $K_{m,\Phi}$, and $[NO]_{\Phi,90}$ were all correlated to lognormal distributions (Fig. 4, *C* and *D*), with median values indicated as 3.8, 23, 110, 8, 50, and 250 nM, respectively. These values correlate well with the predicted values when the median values of the input parameters are used (see above). As a consequence of their high variances, these probability density functions are max-

TABLE 2 Mean and percentile values for output parameters

	Percentile					
Output	Minimum	25%	50% (Median)	Expected Value (Mean)	75%	Maximum
$[NO]_{\Theta,10}$, nM	0.0055	1.0	3.8	19.0	13.0	270.0
$K_{m,\Theta}$, nM	0.05	8.0	23.0	76.0	67.0	1160.0
$[NO]_{\Theta,90}$, nM	0.47	44.0	110.0	270.0	280.0	4210.0
$n_{H,\Theta}$	0.61	1.07	1.32	1.36	1.65	1.97
$[NO]_{\Phi,10}$, nM	0.015	3.6	8.0	19.0	21.0	370.0
$K_{m,\Phi}$, nM	1.1	25.0	50.0	93.0	110.0	1380.0
$[NO]_{\Phi,90}$, nM	11.0	120.0	250.0	470.0	550.0	13,500.0
$n_{H,\Phi}$	0.12	0.92	1.29	1.27	1.65	1.98

imum at X_j values nearly an order of magnitude lower than the medians (i.e., $\ln(X_j)$ is normally distributed, not X_j) (D'Agostino and Stephens, 1986; Silverman, 1986). Nearly 94% of the area under the $f(K_{m,\Theta})$ curve lies in the region where $K_{m,\Theta} < 250$ nM. Hence, despite its high expected value (mean value), 76 nM, the probability that $K_{m,\Theta} < 250$ nM is estimated at more than 90%.

Transient sGC activation

In Fig. 5 is depicted the transient activation of sGC by free NO for the hypothetical activation and deactivation scenarios described above. Activation curves can be characterized by the time is takes to reach ½ of maximum activity, $t_{1/2}$. Note that $t_{1/2}$ is inversely related to k_D and is ≈1.8, 1.7, and 1.0 s for $k_D = 0$, 0.01, and 0.2 s^{-1}, respectively. Figure 5 clearly shows that PSSA can be applied for activation after only 10 s.

For constant k_D, deactivation times are longer, and the difference between activation and deactivation increases substantially as k_D increases. For the deactivation scenarios, $t_{1/2} = 170$, 50, and 3.2 s for $k_D = 0$, 0.01, and 0.2 s^{-1}, respectively. Although deactivation is essentially complete within ~10 s for $k_D = 0.2$ s^{-1}, roughly 3 and 9 min are required to achieve 90% deactivation for $k_D = 0.01$ and 0 s^{-1}, respectively.

Dimensionless representation of the Hill coefficient and Michaelis constant

We characterized the Hill coefficient, $n_{H,\Theta}$, over the range of possible input parameter values by using Eq. 10. $n_{H,\Theta}$ was represented in terms of two dimensionless groups, $\alpha = k_2/(k_D + k_{-2})$ and $\beta = k_3/(K_1(k_D + k_{-2}))$, as illustrated in Fig. 6. The activity of the 6-coordinate sGC complex ($\gamma_{GC6} = k_{GC6}/k_{GC5}$) was varied at three levels: 50% (Fig. 6 *A*), 0% (Fig. 6 *B*), and 100% (Fig. 6 *C*) of full activity. For each plot shown in Fig. 6, diamonds mark the values of α and β evaluated at the median input parameter values (see Table 1).

Because $n_{H,\Theta}$ is very insensitive to γ_{GCB}, we kept γ_{GCB} fixed at its median value in the construction of Fig. 6. Although k_D exerts significant influence on $n_{H,\Theta}$ through the two dimensionless parameters, α and β, the relative sensitivity of $n_{H,\Theta}$ upon ϵ was found to be less than 0.1%, even with k_D at its upper limit. Hence, the dependence of $n_{H,\Theta}$ upon $\epsilon = k_D/k_{-1}$ is minor compared to its dependence on α, β, and γ_{GC6}. We therefore set ϵ at its most likely value, based on the probability distributions summarized in Table 1. The low relative sensitivity of $n_{H,\Theta}$ with respect to ϵ results from its small value. This assumption was confirmed by comparison of the final results (see Fig. 6) with similar results computed for $\epsilon = 0$ (data not shown).

Figure 6 shows that $n_{H,\Theta}$ decreases with k_2 (in most cases), increases with k_3, and decreases K_1. Within the uncertainty range of the dimensionless groups, it is evident that $n_{H,\Theta} \geq 1$, which demonstrates that sGC activation by NO most likely exhibits ultra-sensitive behavior. This result is consistent with results from LHS (Fig. 4 *A*). Around the median value, $n_{H,\Theta} \cong 1.3$, the contours are closely spaced. Thus, in this region, $n_{H,\Theta}$ is relatively sensitive to the input parameters (i.e., small changes in α or β result in large changes in $n_{H,\Theta}$). In contrast, there is a broad region where $n_{H,\Theta} \cong 1$, which becomes even more pronounced as γ_{GC6} increases (compare Fig. 6, *A–C*). Hence, as $n_{H,\Theta} \to 1$, it becomes insensitive to the input parameters.

Figure 7 shows a similar characterization for the apparent Michaelis constant, $K_{m,\Theta}$. In this plot, we kept both K_1 and $\epsilon = k_D/k_{-1}$ fixed at their median values, 0.003 nM^{-1} and 1.5×10^{-5}, respectively, but varied α and β over a wide range. Thus, Fig. 7 is a parametric representation of the dimensionless group, $Y_{m,\Theta}$ (see Eq. 11), which is scaled to the pseudo-Michaelis constant, $K[supstas]_{m,\Theta} = IY_{m,\Theta}/0.003$ nM^{-1}. Although the contour lines are linear on an arithmetic scale, they are displayed on a logarithmic scale to show detail. As in Fig. 6, the diamond denotes the values of α and β at the median input parameter values (see Table 1

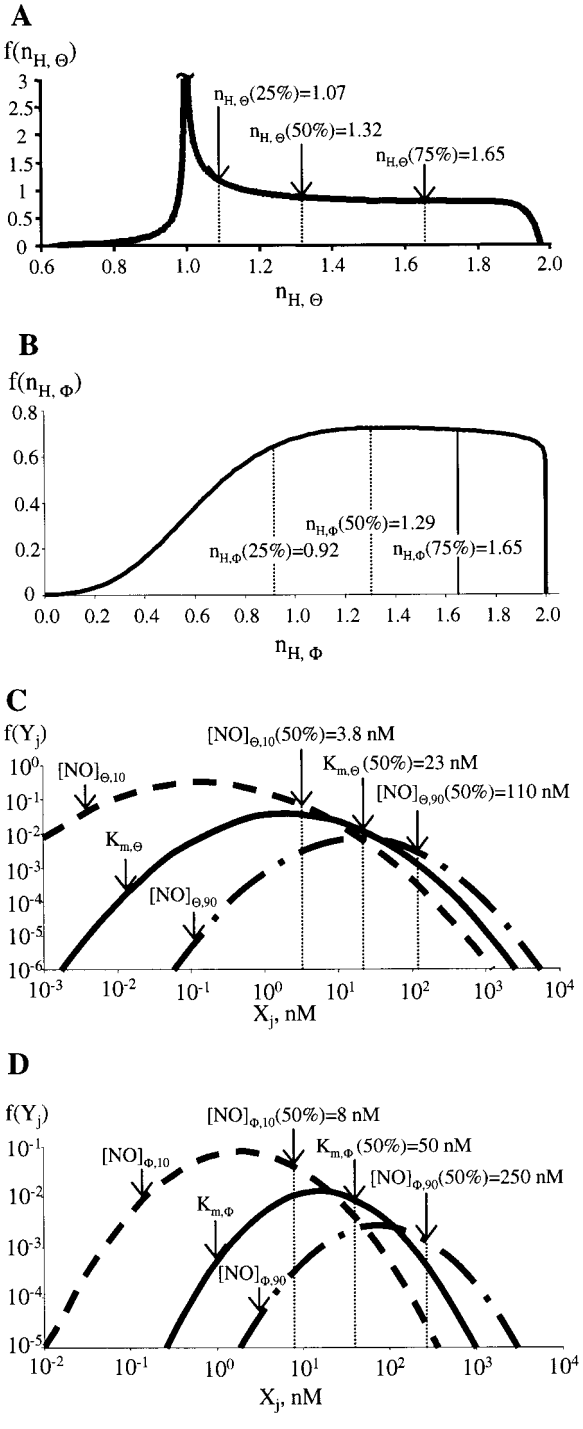

FIGURE 4 Probability density functions, $f(Y_i)$, for the (*A*) output variables $n_{H,\Theta}$; (*B*) $n_{H,\Phi}$; (*C*) $[NO]_{\Theta,10}$ (*dotted line*), $K_{m,\Theta}$ (*solid line*), and $[NO]_{\Theta,90}$ (*dash-dot line*); and (*D*) $[NO]_{\Phi,10}$ (*dotted line*), $K_{m,\Phi}$ (*solid line*), and $[NO]_{\Phi,90}$ (*dash-dot line*). Median and quartile values are indicated with percentiles in parenthesis, as summarized in Table 2.

where $K_{m,\Theta} = 23$ nM). Figure 7 demonstrates that $K_{m,\Theta}$ decreases with both k_2 and k_3, and increases with the quantity, $(k_{-2} + k_D)$.

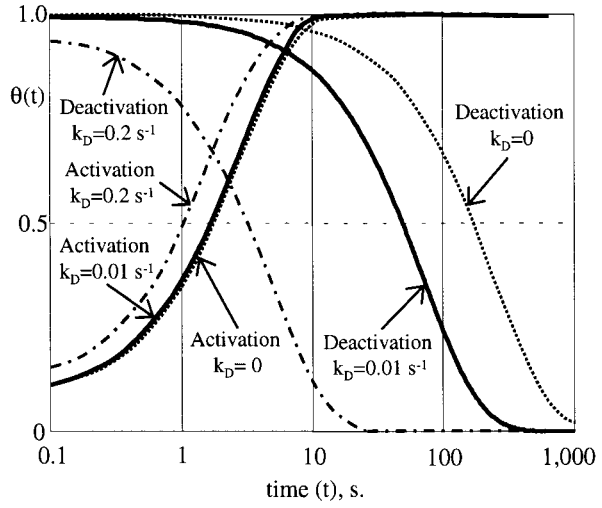

FIGURE 5 Transient activation and deactivation of sGC resulting from an instantaneous change in [NO] (i.e., from [NO] = 0 to 500 nM for sGC activation, and from 500 nM to 0 for sGC deactivation), for $k_D = 0$ (*dotted lines*), $k_D = 0.01\ s^{-1}$ (*solid lines*), and $k_D = 0.2\ s^{-1}$ (*dash-dot lines*). $\theta(t) = (V_{cGMP}(t) - V_{cGMP,B})/(V_{cGMP,500} - V_{cGMP,B})$, where $V_{cGMP,500}$ is the steady-state rate of cGMP formation at [NO] = 500 nM, and $V_{cGMP,B} = k_{GCBE0}$ is the basal cGMP formation rate.

DISCUSSION

sGC activation and inactivation

If free NO regulates sGC activation in vivo, an extrinsic factor must facilitate dissociation of NO from sGC to allow efficacious control of sGC activation. Otherwise, sGC would remain fully activated in vivo, even at low levels of NO. For example, a recent study demonstrated that increasing intracellular calcium concentrations, $[Ca^{2+}]$, inhibits sGC activity in vivo via an noncompetitive mechanism (Parkinson et al., 1999). Increases in $[Ca^{2+}]$ caused both $K_{m,GTP}$ and V_{max} to decrease for both the basal and NO-stimulated forms of the enzyme. Because this regulation mechanism is not yet well understood, additional work is required to assess its impact, but this represents a potential source for $k_{D,obs}$ along with protein thiols and GTP.

The results presented above indicate that $K_{m,\Theta}$ is dependent upon k_D and/or k_{-2}. This lends support to the hypothesis that extrinsic factors, such as intracellular protein thiols, are involved in the regulation of sGC activity. However, the precise mechanism by which these extrinsic factors control sGC activity remains unclear. The median parameter values selected for this study (see Table 1) have assumed that k_D is five-fold larger than k_{-2}, which resulted in relatively higher sensitivities of the outputs to k_D than for k_{-2}. Conversely, if we instead assume that $k_{-2} \gg k_D$, this sensitivity behavior is reversed (data not shown).

PSSA assumes that a continuous supply of NO is available, which maintains [NO] nearly constant within the cell. Thus, if pseudo-steady-state conditions apply, NO con-

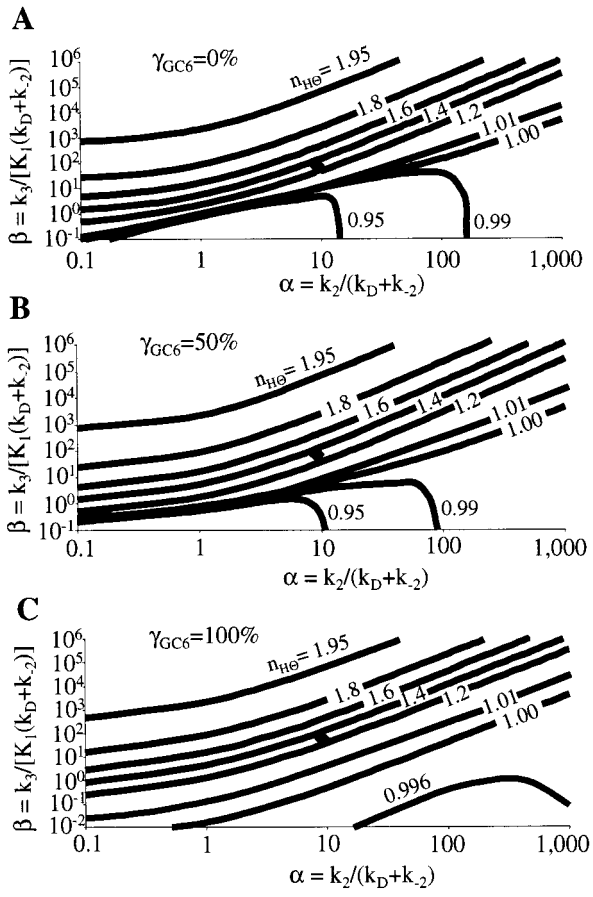

FIGURE 6 Hill coefficient, $n_{H,\Theta}$, for the sGC–NO system as a function of the dimensionless groups, $\alpha = k_2/(k_D + k_{-2})$ and $\beta = k_3/(K_1(k_D + k_{-2}))$, with 6-coordinate sGC complex at (*A*) 50% of k_{GC5}, (*B*) 0% of k_{GC5}, (*C*) 100% of k_{GC5}. ◆, α and β evaluated at the median values (see Table 1).

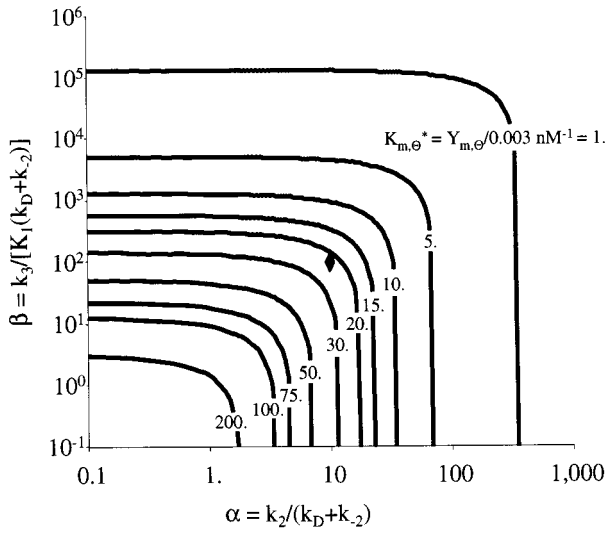

FIGURE 7 Apparent Michaelis constant for cGMP production, $K_{m,\Theta}$, as a function of the dimensionless groups, $\alpha = k_2/(k_D + k_{-2})$ and $\beta = k_3/(K_1(k_D + k_{-2}))$, with 6-coordinate sGC complex at 50% of k_{GC5}. ◆, α and β evaluated at the median values (see Table 1).

sumption does not impact the activity of sGC. In contrast, if a transient pulse of NO is delivered to the cell, [NO] is time dependent, and we observe a much different relationship between $K_{m,\Theta}$ and the kinetic parameters. Therefore, the apparent Michaelis constants and Hill coefficients presented herein should be interpreted as characteristics of sGC activation independent of NO consumption.

Dissociation of NO from sGC reduces the activity of the enzyme (as k_D increases, Θ decreases at fixed [NO]). Furthermore, Fig. 2 *A* illustrates that, for fixed k_D, V_{cGMP} rises from low to maximum activity over a relatively narrow range of [NO], between $[NO]_{\Theta,10}$ and $[NO]_{\Theta,90}$. For $k_D = 0$, 0.01, and 0.2 s^{-1}, respectively, these concentration ranges are ≈2–50 nM, 5–100 nM, and 30–400 nM NO. Figure 2 *B* demonstrates that, for very low or very high [NO], $S^r_{\Theta,[NO]}$ approaches zero. However, at intermediate [NO], $S^r_{\Theta,[NO]}$ is dependent upon k_D and reaches a maximum at some critical value of [NO] (i.e., 2, 10, and 60 nM, for $k_D = 0$, 0.01, and 0.2 s^{-1}, respectively). In addition, Fig. 2 *B* demonstrates that increasing k_D reduces the range of [NO] control (narrower peak), but increases $S^r_{\Theta,[NO]}$ (higher maximum).

As a result of the competing nature of the NO dependent and independent pathways, the effective [NO] window for sGC regulation (i.e., the range of [NO] between 10 and 90% of full sGC activation) can be characterized by the relative values of k_2 and k_3, or by the dimensionless groups, α and β (see Fig. 6). A broader window corresponds to a lower Hill coefficient, $n_{H,\Theta}$. If k_2 dominates over k_3, then $n_{H,\Theta} \rightarrow 1$, corresponding to a broad window. As k_3 increases, $n_{H,\Theta}$ increases, narrowing the window. Therefore, the values of k_2 and k_3 are critical for characterization of sGC regulation by NO.

The 70% probability interval for $n_{H,\Theta}$ is $1.1 < n_{H,\Theta} < 1.5$. In addition, statistical analysis estimates the probability that $n_{H,\Theta} > 1.0$ at nearly 90% (see Fig. 4 *A*). The data depicted in Fig. 6 demonstrate that sGC approaches Michaelis–Menten behavior in a broad domain of α and β, which lies outside the most probable range of the kinetic parameters. We therefore conclude that the "switch" for activating sGC by NO is most likely ultra-sensitive, and sGC is characterized by a narrow window of activation (i.e., $n_{H,\Theta} \geq 1.0$). However, because the distribution function of Fig. 4 *A* shows a high frequency for $n_{H,\Theta} \cong 1.0$, we cannot rule out Michaelis–Menten behavior.

A 5–100-nM range is determined herein for $K_{m,\Theta}$ (see Fig. 7), with a median value of 23 nM (see Table 2). Statistical analysis (see Fig. 4 *C*) estimates more than 90% probability that $K_{m,\Theta}$ is lower than the 250-nM level previously reported (Vaughn et al., 1998a; Stone and Marletta, 1996). In addition, Fig. 7 demonstrates that $K_{m,\Theta}$ exceeds 200 nM only for values of α and β, which lie outside the

most probable range of the kinetic parameters. Hence, in vivo, sGC is activated at much lower levels of [NO] then previously reported and exhibits a $K_{m,\Theta}$ value that is comparable to NO concentrations predicted in arterial smooth muscle (Vaughn et al., 1998a,b). Therefore, previous estimates for the effective distance over which NO can influence the activation of sGC (Vaughn et al., 1998a) need to be re-evaluated. However, future experimental studies are needed with [NO] in the 1–100-nM range to substantiate this hypothesis. In addition, $K_{m,\Theta}$ is strongly dependent upon K_1, which is not well characterized at physiological temperatures.

NO consumption

Experimental data, involving the in situ monitoring of NO release and diffusion through the muscle cells of rabbit aorta (Malinski et al., 1993), has been shown to correlate modestly with first- and second-order rate expressions for NO consumption (Vaughn et al., 1998b). Assuming that NO consumption rates within muscle cells are dominated by the binding of NO to sGC, the results presented herein provide an alternative rate law for NO consumption, which may explain discrepancies in these data. With $k_D \sim 0.01\ s^{-1}$, R_{NO} is approximately first order with respect to NO for [NO] $<$ 1 nM. With [NO] in the range 1–200 nM, the order of NO consumption is in the range 1.5–0, and is zero order as [NO] exceeds 200 nM. Thus, for [NO] $>$ 200 nM, nearly all of the binding sites for sGC are bound with NO, and further consumption of NO is due only to inactivation of sGC (i.e., $R_{max,NO} = (2k_D + k_{-2})E_0$). This is consistent with Fig. 3 *A*, which shows that NO consumption ($\Phi = R_{NO}/R_{NO,max}$) monotonically increases with [NO] independent of k_D, eventually reaching its maximum value, then becoming independent of [NO] at high concentrations. Therefore, as $\Phi \rightarrow 1$, NO consumption is independent of [NO] concentration and the apparent reaction order is zero.

Figure 3 *B*, which plots the logarithmic slope, $S^r_{\Phi,[NO]}$, also shows that as [NO] becomes large, $S^r_{\Phi,[NO]} \rightarrow 0$, independent of k_D. The behavior at lower concentrations is much different. For $k_D > 0$, $S^r_{\Phi,[NO]} \rightarrow 1$ at low concentrations, then passes through a maximum at a critical [NO] before decreasing to zero. The critical [NO] values are 10 and 30 nM, with maximum $S^r_{\Phi,[NO]}$ values of 1.3 and 1.6, at $k_D = 0.01$ and $0.2\ s^{-1}$, respectively. However, for $k_D = 0$, $S^r_{\Phi,[NO]} \rightarrow 2$ as [NO] $\rightarrow 0$, then monotonically decreases over the range 1–1000 nM.

This behavior is the result of the competing nature of the two parallel pathways that lead to the active 5-coordinate sGC complex. As [NO] $\rightarrow 0$ with $k_D = 0$, NO consumption will be controlled by the slow NO-dependent pathway (characterized by k_3), because both the first binding phase (characterized by k_1 and k_{-1}) and the NO independent pathway (characterized by k_2 and k_{-2}) will approach equilibrium at steady state. Thus, as [NO] $\rightarrow 0$ with $k_D = 0$, we observe second-order behavior. However, for $k_D \geq k_{-2}$, dissociation of NO from the E_3 form of sGC controls the NO consumption rate at steady state by displacing the NO-independent pathway from equilibrium. Hence, as [NO] $\rightarrow 0$ with $k_D > 0$, the extent of the NO-dependent pathway becomes negligible, and we observe first-order behavior.

Transient activation and deactivation sGC by NO

Transient simulation of NO binding to sGC (see Fig. 5) indicates that sGC activation occurs much more rapidly than deactivation. In addition, comparison of these results with previously observed in vivo half-lives of 1–2 min (Palmer et al., 1987), suggests that the median value, $k_D = 0.01\ s^{-1}$, is appropriate. Although $t_{1/2}$ was $\sim$60 s for inactivation, which is consistent with the 1–2 min reported for the NO-induced relaxation/contraction of rabbit aorta, additional processes, which were not considered in our analysis, would tend to increase the response time. These processes introduce additional lag times resulting from diffusion of NO to the cell, finite cGMP conversion rates, and other downstream elements of the cGMP signaling cascade.

The proposed mechanism assumes that the observed pseudo-first-order rate constant for NO dissociation is $k_{D,obs} \cong k_D + k_{-2}$. Because available dissociation rate data cannot distinguish between the relative contributions of these two rate constants, we have estimated k_D and k_{-2} based on dissociation rate data in the presence and absence of in vivo cofactors, respectively. The precise sGC deactivation mechanism is not well understood. Hence, an alternative approach is to correlate the output parameters in terms of the observed rate constant, $k_{D,obs} \cong k_D + k_{-2}$, by using a "pseudo-mechanism," in which the fully-activated, E_3, form of sGC was converted to its basal, E_1, form via a first-order process (in other words, set $k_D = k_{D,obs}$ and set $k_{-2} = 0$.). Such a pseudo-mechanism would simplify analysis and may be useful for the correlation of sGC activity with [NO] in vivo; however, it may not accurately depict the precise nature of sGC deactivation and could not be used to predict NO consumption rates.

CONCLUSION

sGC activation and deactivation by NO is likely regulated by interaction with intracellular protein thiols or other cofactors, such as calcium and GTP. Results indicate that the cGMP formation rate reaches 50% of its maximum value for [NO] $<$ 100 nM, with a Hill coefficient in the range 1.1–1.5. Hence, we conclude that sGC can be partially activated at [NO] well below the reported 250 nM, and control of activation is most likely ultra-sensitive. The apparent reaction order for NO consumption via its interaction with sGC is not constant, but varies with [NO]. Future experimental studies should focus on monitoring [NO] lev-

els in vitro, determining chemical equilibrium, using in vivo (37°C) temperatures when possible, and quantifying sGC activity with [NO] in the range 1–100 nM.

This work was supported by grants from the National Science Foundation (BES-9619340) and the National Institutes of Health (R29 HL60636).

REFERENCES

Beckman, J. S., and W. H. Koppenol. 1996. Nitric oxide, superoxide, and peroxynitrite: the good, the bad, and the ugly. *Am. J. Physiol. Cell Physiol.* 271:C1424–C1437.

Brandish, P. E., W. Buechler, and M. A. Marletta. 1998. Regeneration of the ferrous heme of soluble guanylate cyclase from the nitric oxide complex: acceleration by thiols and oxyhemoglobin. *Biochemistry*. 37: 16898–16907.

Bray, H. S. and K. White. 1966. Kinetics and Thermodynamics in Biochemistry, 2nd ed. Academic Press, Inc., New York/London. 52–220.

D'Agostino, R. B., and M. A. Stephens. 1986. Goodness-of-Fit Techniques, Vol. 68. D. B. Owen, editor. Marcel Dekker, Inc., New York, 11–413.

Denninger, J. W., and M. A. Marletta. 1999. Guanylate cyclase and the NO/cGMP signaling pathway. *Biochim. Biophys. Acta.* 1411:334–350.

Doctor, P. G. 1989. Sensitivity and uncertainty analysis for performance assessment testing. *Eng. Geol.* 26:411–429.

Eu, J. P., L. Liu, M. Zeng, and J. S. Stamler. 2000. An apoptotic model for nitrosative stress. *Biochemistry*. 39:1040–1047.

Ferrell, J. E., Jr., and E. M. Machleder. 1998. The biochemical basis of an all-or-none cell fate switch in *Xenopus* oocytes. *Science*. 280:895–898.

Greenwood, P. E., and M. S. Nikulin. 1996. A Guide to Chi-Squared Testing. John Wiley and Sons, Inc., New York. 1–226

Hogg, N., R. J. Singh, and B. Kalyanaraman. 1996. The role of glutathione in the transport and catabolism of nitric oxide. *FEBS Lett*. 382:223–228.

Ignarro, L. J., G. M. Buga, K. S. Wood, R. E. Byrns, and G. Chaudhuri. 1987. Endothelium-derived relaxing factor produced and released from artery and vein is nitric oxide. *Proc. Natl. Acad. Sci. U.S.A.* 84: 9265–9269.

Ignarro, L. J., J. N. Degnan, W. H. Baricos, P. J. Kadowitz, and M. S. Wolin. 1982. Activation of purified guanylate cyclase by nitric oxide requires heme. Comparison of heme-deficient, heme-reconstituted and heme-containing forms of soluble enzyme from bovine lung. *Biochim. Biophys. Acta.* 718:49–59.

Ignarro, L. J., R. G. Harbison, K. S. Wood, and P. J. Kadowitz. 1986. Activation of purified soluble guanylate cyclase by endothelium-derived relaxing factor from intrapulmonary artery and vein: stimulation by acetylcholine, bradykinan and arachiodonic acid. *J. Pharmacol. Exp. Ther.* 222:893–900.

Kharitonov, V. G., G. M. Russwurm, D. Magde, V. S. Sharma, and D. Koesling. 1997a. Dissociation of nitric oxide from soluble guanylate cyclase. *Biochem. Biophys. Res. Commun.* 239:284–286.

Kharitonov, V. G., V. S. Sharma, D. Magde, and D. Koesling. 1997b. Kinetics of nitric oxide dissociation from five- and six-coordinate nitrosyl hemes and heme proteins, including soluble guanylate cyclase. *Biochemistry*. 36:6814–6818.

Koshland, D. E., Jr.1998. The era of pathway quantification. *Science*. 280:852–853

Magulis, A. and A. Sitaramayya. 2000. The rate of deactivation of nitric oxide-stimulated soluble guanylate cyclase: influence of nitric oxide scavengers and calcium. *Biochemistry.* 39:1034–1039.

Makino, R., H. Matsuda, E. Obayashi, Y. Shiro, T. Iizuka, and H. Hori. 1999. EPR characterization of axial bond in metal center of native and cobalt-substituted guanylate cyclase. *J. Biol. Chem.* 274:7714–7723.

Malinski, T., Z. Taha, and S. Grunfeld. 1993. Diffusion of nitric oxide in the aorta wall monitored in situ by porphyrinic microsenors. *Biochem. Biophys. Res. Commun.* 193:1076–1082.

McKay, M. D., R. J. Beckman, and W. J. Conover. 1979. A comparison of three methods for selecting values of input variables in the analysis of output from a computer code. *Technometrics*. 21:239–245.

Mendenhall, W., and R. L. Scheaffer. 1973. Mathematical Statistics with Applications. Duxbury Press, North Scituate, MA. 1–553, A24.

Palmer, R. M. J., A. F. Ferrige, and S. Moncada. 1987. Nitric oxide release accounts for the biological activity of endothelium-derived relaxing factor. *Nature*. 327:524–526.

Parkinson, S. J., A. Jovanovic, S. Jovanovic, F. Wagner, A. Terzic, and S. A. Waldman. 1999. Regulation of nitric oxide-responsive recombinant soluble guanylyl cyclase by calcium. *Biochemistry*. 38:6441–6448.

Silverman, B. W. 1986. Density Estimation for Statistics and Data Analysis. Chapman and Hall, Ltd., New York/London. 1–147

Stone, J. R., and M. A. Marletta. 1994. Soluble guanylate cyclase from bovine lung: activation with nitric oxide and carbon monoxide and spectral characterization of the ferrous and ferric states. *Biochemistry*. 33:5636–5640.

Stone, J. R., and M. A. Marletta. 1995. Heme stoichiometry of heterodimeric soluble guanylate cyclase. *Biochemistry*. 34:14668–14674.

Stone, J. R., and M. A. Marletta. 1996. Spectral and kinetic studies on the activation of soluble guanylate cyclase by nitric oxide. *Biochemistry*. 35:1093–1099.

Stone, J. R., and M. A. Marletta. 1998. Synergistic activation of soluble guanylate cyclase by YC-1 and carbon monoxide: implications for the role of cleavage of the iron–histidine bond during activation by nitric oxide. *Chem. Biol*. 5:255–261.

Stryer, L. 1995. Biochemistry. W. H. Freeman, New York. 147–200

Tomita, T., T. Ogura, S. Tsuyama, Y. Imai, and T. Kitagawa. 1997. Effects of GTP on bound nitric oxide of soluble guanylate cyclase probed by resonance Raman spectroscopy. *Biochemistry*. 36:10155–10160.

Vaughn, M. W., L. Kuo, and J. C. Liao. 1998a. Effective diffusion distance of nitric oxide in the microcirculation. *Am. J. Physiol. Heart Circ. Physiol.* 274:H1705–H1714.

Vaughn, M. W., L. Kuo, and J. C. Liao. 1998b. Estimation of nitric oxide production and reaction rates in tissue by use of a mathematical model. *Am. J. Physiol. Heart Circ. Physiol.* 274:H2163–H2176.

Wink, D. A., and J. B. Mitchell. 1998. Chemical biology of nitric oxide: insights into regulatory, cytotoxic, and cytoprotective mechanisms of nitric oxide. *Free Radical Biol. Med*. 25:434–456.

Wong, P. S., J. Hyun, J. M. Fukuto, F. N. Shirota, E. G. DeMaster, D. W. Shoeman, and H. T. Nagasawa. 1998. Reaction between S-nitrosothiols and thiols: generation of nitroxyl (HNO) and subsequent chemistry. *Biochemistry*. 37:5362–5371.

Zhao, Y., P. E. Brandish, D. P. Ballou, and M. A. Marletta. 1999. A molecular basis for nitric oxide sensing by soluble guanylate cyclase. *Proc. Natl. Acad. Sci. U.S.A.* 96:14753–14758.

Zhao, Y., C. Hoganson, G. T. Babcock, and M. A. Marletta. 1998a. Structural changes in the heme proximal pocket induced by nitric oxide binding to soluble guanylate cyclase. *Biochemistry*. 37:12458–12464.

Zhao, Y., and M. A. Marletta. 1997. Localization of the heme binding region in soluble guanylate cyclase. *Biochemistry*. 36:15959–15964.

Zhao, Y., J. P. M. Schelvis, G. T. Babcock, and M. A. Marletta. 1998b. Identification of histidine 105 in the beta 1 subunit of soluble guanylate cyclase as the heme proximal ligand. *Biochemistry*. 37:4502–4509.